TECHNICAL MEMORANDUM

X-391

HEAT TRANSFER TO BLUNT AXIALLY SYMMETRIC BODIES

By John O. Reller, Jr.

Ames Research Center
Moffett Field, Calif.

NATIONAL AERONAUTICS AND SPACE ADMINISTRATION

WASHINGTON

September 1960

NATIONAL AERONAUTICS AND SPACE ADMINISTRATION

TECHNICAL MEMORANDUM X-391

HEAT TRANSFER TO BLUNT AXIALLY SYMMETRIC BODIES*

By John O. Reller, Jr.

SUMMARY

A large number of bodies of revolution were tested to determine the effects of variations in body shape on over-all heat-transfer rates. Included in the investigation were studies of the effects of changes in body fineness ratio, ratio of nose to base diameters, and nose profile - including the addition of spikes. The test ranges of nose to base diameter ratios and body fineness ratios were, respectively, 0 to 1 and 0.3 to 2.0. Tests were conducted at Mach numbers from 3.0 to 6.3, Reynolds numbers from 2.5 to 0.4 million based on body diameter, and stagnation temperatures from 530° R to 840° R.

Heat-transfer data for blunt shapes with laminar flow expressed as the Stanton number times the square root of Reynolds number (based on conditions behind a normal shock) were essentially independent of free-stream Mach number and body shape within the range of the present investigation. The addition of nose spikes resulted in substantial increases in heat transfer for both steady and unsteady flows. A comparison of some of the test results with theoretical estimates of heat-transfer rates showed relatively good agreement.

INTRODUCTION

It is known that blunting of body noses and wing leading edges can result in appreciable reductions in the aerodynamic heating rates of the forward portions of vehicles, either during entry into the earth's atmosphere at high velocities (see, e.g., ref. 1) or in steady flight at hypersonic speeds. It is therefore of interest to inquire into the type of blunt profile and the amount of bluntness, relative to maximum body diameter or wing thickness, that will be most effective in minimizing convective heat-transfer rates. There are, of course, requirements other than that of minimum heat transfer which must be considered in the design of high-speed vehicles. For example a large degree of

*Title, Unclassified

bluntness is not compatible with the requirement of low drag for long-range aircraft operating within the earth's atmosphere, while, on the other hand, structural design and surface cooling techniques may be simplified by bluntness.

The purpose of the present paper is to compare the heat-transfer rates to a variety of blunt bodies of revolution and to evaluate, in part, the effects of body-nose geometry on heat-transfer rates. The comparable two-dimensional problem and other possible aerodynamic considerations are not included in the discussion. The bodies included in the study range from large-angle cones to fully blunt cylinders and include shapes with varying sizes of blunt noses, varying fineness ratios and varying nose profiles - some with nose spikes. The experimental heat-transfer results and some corresponding pressure-distribution data were obtained in the Ames 10- by 14-Inch Supersonic Wind Tunnel at Mach numbers from 3.0 to 6.3 with corresponding free-stream Reynolds numbers from 2.5 to 0.4 million based on body diameter.

SYMBOLS

A reference area

B.L. boundary layer

c_p specific heat at constant pressure

D diameter of body base

d diameter of body nose

h convective heat-transfer coefficient

h_l local convective heat-transfer coefficient

K parameter fixing level and gradient of body surface pressure coefficients (see ref. 2)

L body length

M Mach number

p static pressure

q dynamic pressure

Q heat-transfer rate

R Reynolds number referenced to body base diameter, $\frac{\rho_\infty U_\infty D}{\mu_\infty}$

R_s Reynolds number based on distance along surface from stagnation point, $\frac{\rho_\infty U_\infty S}{\mu_\infty}$

S distance along surface from stagnation point

St Stanton number

T static temperature

T_r reference temperature

T_w wall temperature

U velocity

$\bar{x},\bar{r}$ cylindrical coordinates of body profile normalized by body nose radius

ρ density

μ coefficient of viscosity

Subscripts

∞ free-stream conditions

1 local flow conditions at edge of boundary layer

ns conditions behind normal shock wave

b body base area

a body surface area exclusive of the base

EXPERIMENT

Test Models

Profiles of the bodies of revolution tested in this investigation are shown in figure 1, where related shapes are superposed. The variations in body fineness ratio and in nose to base diameter ratio were from 0.3 to 2.0 and from 0 to 1, respectively. The hemisphere cones of fixed fineness ratio and variable nose diameter and the

truncated cones of groups 1 and 2 (fig. 1(a)) were tested to determine the effects on heat-transfer rates of the variation of nose diameter relative to base diameter and the effects of changing the nose profile shape from flat to spherical. The K-series bodies of group 3 (fig. 1(b)) are also shapes of fixed fineness ratio and variable nose diameter. The profile shapes of this group of bodies are based on the premise that the heat-transfer rates may be reduced by obtaining low stream velocities in the high-density flow at the nose and, conversely, low air densities in the high-velocity flow over the afterportions of the bodies, as described in reference 2. The equation defining the profile shapes of the K-series bodies is (see ref. 2)

$$\bar{x} = \int_1^{\bar{r}} \sqrt{(\bar{r})^K - 1}\, d\bar{r}$$

The K-series bodies of group 4 (fig. 1(b)) were tested to determine the effect of variation of the fineness ratio of bodies having a fixed ratio of nose to base diameters. The profile shapes of these bodies are also defined by the equation above. It may be noted that the K-6 body shape is common to both groups 3 and 4 and therefore provides a basis for comparison between the effects of variable nose to base diameter ratio and variable fineness ratio.

Some variations of nose profile shape were investigated by tests on the bodies of group 5 (fig. 1(c)). The basic flat-nose shape of this group is the K-6 body shape of groups 3 and 4. The profiles of the noses of this group of bodies are essentially circular segments of varying radii of curvature.

The three bodies of group 6 (fig. 1(d)) - 60° cone, hemisphere cone and hemisphere - were tested to establish comparative levels of heating of simple, basic shapes. As in reference 2 these bodies are used here as reference shapes. The two bodies of group 7 provide a comparison of heat-transfer rates to two different truncated conical shapes of approximately equal surface area (exclusive of base area).

The bodies of group 8 (fig. 1(e)) with nose spikes were tested to establish the effects of various nose spikes on over-all heat-transfer rate. The bodies shown in figure 1(f) are segments of the K-6 shape of group 4, which were used to measure heating rates to the flat face and the shoulder region.

Heat-transfer models were made of anodized aluminum with surface finishes of the order of 10 to 20 microinches. The pressure-distributio model, K-6 shape, was made of polished steel and had a somewhat smoother surface than did the heat-transfer models.

Apparatus and Test Procedure

Tests were conducted in the Ames 10- by 14-Inch Supersonic Wind Tunnel at Mach numbers from 3.0 to 6.3, corresponding Reynolds numbers from 2.5 to 0.4 million, and stagnation temperatures from 530° to 840° R. Details of the heat-transfer apparatus are shown in figure 2. Heat-transfer models were supported from the rear by a thin cylindrical shell that was shielded from the air stream. An outer concentric shield was separated from the thin shell and the model by an air gap. Heat input was through a resistance heater of Inconel wire wound on a copper spool located at the forward end of the support shell. A guard heater and a temperature equalizing ring were attached to the support shell and were used to stop the rearward heat flow through the shell and thus prevent heat loss to the support system. Heat-transfer instrumentation consisted of two iron-constantan thermocouples soldered to the front heater spool, two differential thermocouples on the support shell to indicate the temperature balance between the front and rear heaters, and from three to seven iron-constantan thermocouples pinned within the test models at various points near the outer surface. Temperatures were measured on a self-balancing precision potentiometer while the heat-transfer rate was determined for steady-state conditions from the electrical power input to the heater. Data were recorded for the no-heat-flow condition and at several heat-transfer rates with front to rear heater-temperature balance. Maximum model temperatures ranged from 30° F to 90° F above that for the no-heat-flow condition.

Pressures were measured with conventional U-tube manometers filled with mercury and dibutyl for high and low absolute pressures, respectively.

Reduction and Accuracy of Data

The experimental data of this investigation are representative of convective heating rates for an isothermal surface, near recovery temperature in an ideal-gas flow. (These results can be compared with the theoretical predictions of reference 3 if a measured pressure distribution is used to define local Mach numbers.) Radiant-heating effects have been neglected since model-surface and tunnel-wall temperatures were very nearly the same. This relatively simple experimental technique, that is, using a solid model of high conductivity, results, of course, in the determination of over-all heating rates. This rather gross approach can be partially refined by testing solid sections of bodies that are isolated from the remainders, as was done in the case of the K-6 shape.

The steady-state heat-transfer measurements were reduced in the following manner. The convective heat-transfer coefficient is defined as:

$$h = \frac{Q}{A(T_w - T_r)}$$

where Q is the electrical power to the heater, A is a reference area, and $T_w - T_r$ is the difference between the wall temperature and a reference temperature. The reference temperature T_r is not a direct experimental measurement, although it is close to the body temperature at the minimum Q condition for which temperature balance was obtained between main and guard heaters. This temperature T_r is the $Q = 0$ intercept obtained by extrapolation of the measured Q (isothermal surface) versus T_w data, based on the assumption that for a laminar boundary layer, the heat-transfer coefficient, h, is a constant for small values of the temperature potential, $T_w - T_r$. A similar assumption was made for models tested with fixed transition. For variable transition location the temperature potential was based on model temperature for the no-heat-loss test condition. Heat-transfer coefficients were converted to Stanton numbers,

$$St = \frac{h}{(\rho U c_p)_\infty} = \frac{Q}{A(T_w - T_r)(\rho U c_p)_\infty}$$

where St_a and St_b are referred to the forebody surface area and base area, respectively.

The estimated accuracies of the experimental data are listed as follows:

Heat-transfer coefficient, h	±10 percent
Stanton number, St	±13 percent
Reynolds number, R	±1.5 percent

These estimates do not include the effect of local deviation from the isothermal condition on boundary-layer development and heat capacity. This effect is considered to be small, however, since the deviations from uniform surface temperature varied from ±1° F to ±3° F in the tests. In addition, the experimental heat-transfer coefficients include a contribution due to heat transfer from the bases of the models. Models of 2-, 2-1/4-, and 3-inch diameter were tested and only a center region, 1.8 inches in diameter, was shielded. Thus, depending on model diameter, 16, 34, and 63 percent, respectively, of the base area was exposed. The heat-transfer contribution of the exposed base was estimated to be less than 6 percent of the total in all cases.

Furthermore, it should be noted that all of the models in each group, except groups 7 and 8, had the same base diameter; thus the relative effects of base heating would be nearly constant in each group. For this reason, comparisons of relative heat-transfer chracteristics in each group are not greatly affected by base heating.

RESULTS AND DISCUSSION

Effects on Heat-Transfer Rate of Variations of Body-Shape Parameters

Size of nose relative to body base.- Some effects of body nose size on the rates of heat transfer to blunt shapes of constant fineness ratio are shown in figure 3 where Stanton number is shown relative to the ratio of body nose to base diameter. The test results are for laminar boundary-layer flow, and show that heating rates are relatively insensitive to nose diameter. It can be seen that the heat-transfer rate per unit base area, St_b, for bodies with equal base diameters is apparently a minimum for ratios of nose to base diameters of about 0.2 (fig. 3(a)) while the rate per unit surface area, St_a, is a minimum for ratios of d/D from about 0.8 to 1.0 (fig. 3(b)). It can be shown that, for these test results, the minimum heat-transfer rate per unit volume occurs at values of the diameter ratio of about 1.0. Comparative data for bodies with approximately equal surface areas are shown in table I where Stanton numbers for a 60° cone and a 60° hemisphere cone are listed. In this case, as in the case of fixed fineness ratio, it is evident that a small amount of blunting is generally favorable throughout the range of test Mach numbers. The very large reduction in heat-transfer rate at $M_\infty = 3.5$ is associated with the effect of the body-nose shape on the character of the boundary layer over the afterportion of the body as will be discussed in a later section.

On the basis of the data shown in figure 3 and in table I, therefore, it is evident that while a small amount of bluntness is beneficial in reducing the level of total heating to shapes of a given fineness ratio, the increased nose size and the increased body surface area associated with greater bluntness result in increasing total heat inputs. Of course, if heat-input rates per unit surface area or per unit volume are important in a vehicle design, the larger degrees of bluntness may be advantageous. It should be noted, of course, that with increasing nose bluntness a greater portion of the total heat input is into the nose regions of bodies of given fineness ratio, and the average rates over the afterportions are decreased as a result of the decreased body slopes relative to the free-stream direction.

Fineness ratio.- The effect on heat-transfer rates of variations of body fineness ratio for bodies with fixed ratios of nose to base

diameters is shown in figure 4. Estimated values of the heating rates for a flat surface (L/D = 0) were based on measured rates to the flat-faced model segment shown in figure 1(f). The curves for the K-series bodies were extended to these values. It can be seen in figure 4(a) that fineness ratio has a relatively small effect on Stanton number, St_b, in particular for body length to base diameter ratios from 0.5 to 2. By comparison, in figure 4(b), Stanton number St_a decreases markedly as a result of the increase of surface area with increasing fineness ratio. The general trends of the changes in Stanton number with fineness ratio may be seen to be somewhat similar to the measured and calculated variations for laminar flow over cones.

Body-nose shape.- The shape of a body nose and the profile shape at the junction of nose and afterbody can affect heat-transfer rates in two fashions. First, the local heating rates over the nose and shoulder regions are to a large degree, dependent on local radii of curvature, that is, on the detailed shape of the nose and shoulder. Second, as pointed out in reference 4, the shoulder profile may be such as to induce transition from laminar to turbulent flow in the boundary layer and thus increase heat-transfer rates over much of the afterbody. The first effect was investigated by varying the shape of the nose of a basic K-6 body, while holding the shoulder radius constant. The models are shown as group 5 in figure 1, and the results are presented in figure 5. All profiles were spherical sectors and the depth or height was referenced to the location of the flat face. Data were obtained only at $M_\infty = 4.24$ and zero angle of attack. It can be seen in figure 5 that the minimum Stanton number occurred at a cavity depth ratio of about 0.08. As cavity depth ratio was increased from 0.08 to 0.24 the Stanton number increased in a regular manner. However, at a depth ratio of 0.36 the flow in the cavity and over the shoulder exhibited a random unsteadiness of large magnitude, and a substantial increase in heating rate was measured. Two shadowgraph pictures of this unsteady flow are shown in figure 6. This phenomenon is the same as that reported in reference 5 for a hemispherical cavity. The data of reference 5 show local heating rates with unsteady flow in the cavity to be, in some cases, of the order of two to three times those at corresponding points on a convex hemispherical nose. It was noted, however, that a small angle of attack ($\sim 2^\circ$) was sufficient to establish a steady-flow, low-heating-rate situation. For the present data at zero angle of attack, the comparable results are similar in that the total-heat rate to this body, in the unsteady-flow situation, is greater than that estimated for the basic shape with essentially a full hemispherical nose as shown in figure 5. In all probability the heating rates to the nose alone would differ by a much larger percentage.

The second effect, that of nose and shoulder shape on boundary-layer transition, is illustrated in figure 7 where Stanton numbers are shown for one fineness-ratio-2 hemisphere cone and several truncated cones (groups 1 and 2). The data are for $M_\infty = 3.5$, where

Reynolds numbers are sufficiently high to illustrate this effect. Curves are faired through the truncated-cone data which represent heat-transfer rates with partly turbulent boundary-layer flow over the models. The hemisphere-cone group is represented by the data at $d/D = 1/2$ and, of course, by that at $d/D = 0$ which is a limiting case common to both groups. On the assumption that the trend with d/D for a hemisphere cone with laminar boundary layer will be similar to that at $M_\infty = 5$, shown in figure 3, the heating rate at $d/D = 1/2$ is representative of the level of heating over a considerable range of nose to base diameter ratios. On this basis, it is seen that for the test conditions at $M_\infty = 3.5$, the heat-transfer rates for the flat-nosed bodies can be as much as twice those for the round-nosed bodies in spite of the fact that the heat input to a flat nose has been shown (ref. 5) to be less than that to a hemisphere of the same diameter. The relative magnitude of this effect of nose or shoulder shape is dependent to a large degree, of course, on body fineness ratio and on the size of the body nose relative to the body base. This latter factor determines, in part, the rate of heat transfer to the afterbody relative to that to the nose.

The test results at $M_\infty = 3.5$ shown in table I are similar in nature to those discussed above; that is, the spherical-nosed model had a greater extent of laminar flow than did the cone body. The large difference in total heat-transfer rates that may be seen in table I is of the same magnitude as that shown in figure 7.

Nose spikes.- Theoretical and some experimental investigations, reference 6 for example, have indicated significant reductions in heat-transfer rates in regions of separated flow. Thus, there exists the attractive possibility of reducing the heating rate to a blunt nose by using a nose spike to create a laminar separated region. Investigations of this effect in air flow at Mach numbers from 1.7 to 5.0 and $M_\infty = 6.8$ are described in references 7 and 8, respectively, while a similar investigation in $M_\infty = 14$ helium flow is reported in reference 9. Furthermore, in reference 10, it was shown that a nose spike can produce an unsteady flow in which the recovery factors over the majority of a body are well below normal values for a turbulent boundary layer. This latter effect, then, might lead to a reduction in heating rates to body surfaces normally enveloped in turbulent boundary-layer flow. A brief survey of these possibilities was included in the present investigation, the results of which are shown in figure 8.

In figure 8 the lower curve is the variation of Stanton number with Mach number for the basic K-6 body. A single flagged point at $M_\infty = 4.24$ is for a flat-faced cylinder of the same fineness ratio. The upper curve represents the results with various length spikes. (Spike diameter and tip shape are not critical for the sizes chosen, at least for the unsteady type of flow discussed in ref. 10.) The triangular symbols shown at $M_\infty = 5$ and 6.3 are for a long spike with

steady separated flow at free-stream Reynolds numbers representative of fully laminar boundary layer on the unspiked reference model. This spiked configuration has considerably higher heating rates than the reference model, although the percentage increase is less at the higher Mach number. These measured increases in heating rate are in agreement with those reported in reference 7 but are in opposition to the results of reference 9, where a spike of about the same length (relative to nose diameter) caused a 25-percent decrease in heating rate. The probable reason for this lack of agreement with the results of reference 9 is the difference in test Mach and Reynolds numbers. The results of reference 8 show that local heating rates on a blunt face are strongly influenced by the laminar or turbulent nature of the separated free boundary ahead of the blunt face, and that transition Reynolds numbers for this boundary may be considerably below those for attached laminar flow. This latter finding of free boundary transition at relatively low R is also indicated on shadowgraph pictures of the present tests. At $M_\infty = 6.3$ the laminar free boundary approaches the shoulder of the body, which could explain the relatively smaller increase in heating rate shown in figure 8. Thus the present results are considered to be consistent with those of references 8 and 9, which indicate over-all reductions in heating rates at high Mach numbers and/or sufficiently low Reynolds numbers.

Turning now to the shorter spikes which caused large-scale unsteady flow to envelop the body it is seen that Stanton numbers, relative to those for attached laminar flow, are increased by a factor of from 2-1/2 at $M_\infty = 3$ and $R = 2.05 \times 10^6$ to about 1-1/2 at $M_\infty = 6.3$ and $R = 0.38 \times 10^6$. Spike-tip shape apparently made little difference, whether sharp or blunt. Furthermore, at $M_\infty = 4.24$ the heating rate with unsteady flow is shown to exceed that for the K-6 body with turbulent afterbody flow. This latter value is indicated by the filled symbol in figure 8 and was obtained by using a boundary-layer trip at the shoulder of the model. Thus, at the Mach numbers and Reynolds numbers of these tests at least, the use of short spikes that produce unsteady flow does not appear promising for the reduction of heat-transfer coefficients on low-fineness-ratio blunt bodies. It should be remembered, of course, that heat rate, Q, depends both on the heat-transfer coefficient and the temperature potential. The lower recovery factors associated with short spikes in the discussion of reference 10 (which indicate reduced temperature potentials), when considered with a Stanton number ratio (the ratio of Stanton number with spike to that without spike) that is decreasing with Mach number as shown in figure 8, may at higher Mach numbers and/or lower Reynolds numbers result in heating rates to a blunt shape which are less than those for attached turbulent boundary-layer flow.

Variation of Heat-Transfer Rates With Mach Number

The variation with free-stream Mach number of heat-transfer results for a representative group of shapes is presented in figure 9. It is evident that the large increase of Stanton number with M_∞ is common to those shapes having laminar boundary-layer flow. The test results for the 60° cone at Mach numbers of 3.0 to 3.5 and for the hemisphere cone at Mach number 3.0 shown in figure 9 are higher than those for the other test bodies because turbulent rather than laminar flow existed over portions of their surfaces. The theoretical curve shown is that calculated for laminar flow by the method of reference 11 and by use of the transformation from flat-plate to conical flow.

It would be expected that the variation of Stanton number shown is due both to the effects of changing Mach number and to the effect of Reynolds number as it varies with Mach number in the wind tunnel. It is known that, for laminar flows, Stanton number varies inversely with the square-root of Reynolds number and it is expected that, for blunt shapes, if the Reynolds number were based on conditions behind the normal shock wave, the effects of free-stream Mach number variations might be largely eliminated. Some of the present results modified in this manner are shown in figure 10 where the variation with test Mach number of Stanton number multiplied by $\sqrt{R_{ns}}$ is shown for the test bodies with laminar boundary-layer flow. The theoretical results shown are the same as those shown in figure 9 for a 60° cone.[1] It is particularly interesting to note that the data correlate well for these shapes despite the fact that a substantial portion of the heat transfer occurs over the afterportion of the bodies. This result indicates that, at least within the boundary layer, the total pressure loss through the shock wave influences the flow well aft on the bodies.

Local Heat-Transfer Rates

The measurement of over-all heat-transfer rates described herein can, at best, give only a qualitative idea of local heating rates. For most of the simpler shapes, of course, good estimates of local heating rates can be obtained with existing theories if the boundary layer flow is assumed to be laminar. Some difficulty is encountered, however, for flat-nosed shapes with afterbody curvature and relatively high local pressure gradients. In reference 2 a limited comparison was made between local heating rates (integrated over portions of the body surface)

[1]The results for the 60° cone have been presented in this same form, that is, $St_b \sqrt{R_{ns}}$, since this shape could be considered a blunt body even though it has an attached oblique shock wave.

calculated using the method of Stine and Wanlass (ref. 3) and experimental data for the K-6 shape shown in figure 1. These theoretical distributions are reproduced in figure 11, along with theoretical stagnation region values calculated by the method of Sibulkin (ref. 12) and two-dimensional distributions calculated by the method of Van Driest (ref. 11) for the same local flow conditions and with Reynolds numbers based on the surface distance from the stagnation point. Experimentally determined surface-pressure distributions were used in calculating these heating-rate distributions. In each case, a portion of the Stine-Wanlass distribution curve is shown as a dashed line in the shoulder region to indicate a measure of uncertainty in the theoretical estimates. The magnitude and the location of the maximum points are uncertain because of the spacing of the pressure taps and the extrapolation required in the application of the theoretical method. In any event, it is obvious that a region of high heating rates exists on the shoulder and that, over most of the afterbody, heating rates are much less than 1/2 the stagnation point value. This trend is compared with a theoretical heat-rate distribution for the 60° cone at $M_\infty = 5$, in figure 11(c). The main feature of this comparison is the shift of the critical heating region from the point of the cone, where the surface area is small, to the shoulder of the body where the surface area is relatively large. The effect of this shift is to counterbalance the reduced heating rates over the rear portion of the K-6 shape. This fact is verified by the experimental data of figure 9 which show that the heating rate for the K-6 shape is not much less than for the 60° cone. Thus, it is obvious that a corner with enough curvature to forestall premature transition may still be subjected to very high heating rates. This effect suggests the desirability of a more refined design approach. One obvious change is to use a slightly convex face which would tend to reduce the local density and heat rate at the shoulder, at the expense of an increased heat rate to the stagnation region. Such a refinement is represented by the theoretical estimates in figure 11(a) and by the experimental data point in figure 5, for the model with a nose cap height of 0.07 of the nose diameter. The theory, as expected, indicates a reduction in heating rate at the shoulder and an increase over the center of the nose; both the integrated theoretical value and the test point shown in figure 5 indicate a slight net increase in total heating. Thus, the best compromise between nose and shoulder heating is not obvious from this limited information. It is of interest to observe, however, that the nose curvature of this configuration is nearly the same as that which resulted in the minimum total heat rate to hemispherical segments as noted in reference 5.

In figure 12, integrated values of theoretical heat-transfer coefficients for portions of the body surface, obtained from the distributions of figure 11, are compared with separate experimental measurements of heating rates for these same surfaces. The experimental data were obtained by measuring the heating rates to the body segments

shown in figure 1(f) and in the small sketches in figure 12. Theory and experiment are seen to be in reasonably good agreement. However, a comparison of theory and experiment for the flat nose and for the nose-plus-shoulder test bodies indicates that the theory overestimates heating rates in the region of high pressure gradients. This observation is consistent with the fact that the theories of Lees (ref. 13) and Cohen and Reshotko (ref. 14) indicate smaller changes in local heating rates in regions of substantial pressure gradient than does the method of Stine and Wanlass.

Summary of Present Results

The over-all response of aerodynamic heating rates for laminar boundary-layer flow to changes in body shape are summarized in figure 13. The data are presented in a generalized form as the variation of $St\sqrt{R_{ns}}$ with fineness ratio, L/D. In figure 13(a), the heating rates per unit base area are shown. Also shown are the heating rates estimated by a simple cone theory, the theoretical value for a flat face, and a semiempirical variation for hemisphere-cylinder bodies based on the measured hemisphere data. The bracketed data are representative of the range covered by the K-series and hemisphere-cone groups of bodies. It is apparent that the largest increase in heating rate occurs between $L/D = 0$ and 0.5. Since the estimate for the flat-faced model at $L/D = 0$ is also a limiting value for cones, theory indicates a minimum in heat transfer to cones between $L/D = 0$ and 0.2. It is possible that a similar minimum would occur for a very blunt K-series shape, although this fact has not been demonstrated. The theory for cones also indicates a maximum in the vicinity of $L/D = 1/2$. In the L/D range from 1/2 to 1 a cone has about the same heating rate as a variety of very blunt shapes. However, a small amount of spherical tip blunting results in a marked reduction in heating rate on a conical shape in this L/D range, as has been shown previously by use of the data in table I. Near $L/D = 2$ the heat transfer to a cone is not reduced as much by small blunting although its heating is far below that for the bluntest shapes. It is indicated that, for a given fineness ratio, shapes that have minimum surface area and that utilize a normal bow shock to reduce the energy level of the air in contact with the surface will have the lowest total heating rates per unit base area.

In figure 13(b) the same data are replotted in a form that is indicative of the variation of heating rates over afterbody surfaces with increasing body fineness ratio. (For cones the theory again indicates a maximum at L/D of about 1/2.) The heat transfer to the blunter shapes, as would be expected, decreases rapidly with increasing L/D since afterbody surfaces are less steeply inclined to the stream and/or are enveloped in the relatively high-entropy air flow passing through the strong bow shock wave. The data fall in a rather well

defined band, within which a given heat-transfer rate may be obtained for a variety of shapes. At an L/D of about 0.8 the heating rate (with laminar boundary-layer flow) is decreased, by increasing bluntness, down to the minimum value for a fully blunt cylinder. Thus, in a situation where body volume is an important factor, these results indicate minimum heat load per unit volume for very blunt shapes of relatively high fineness ratio. If laminar boundary layer is assured and local "hot spots" can be tolerated, a shape that approaches a full cylinder appears most favorable. Shapes similar to the blunter K-series bodies are in this category and have, as well, the advantage of promoting laminar boundary-layer flow.

CONCLUSIONS

The convective heat-transfer rates of various blunt shapes of fineness ratios from 0.3 to 2 were determined in an ideal gas flow at Mach numbers from 3 to 6 and Reynolds numbered (based on model diameter) from 0.4×10^6 to 2.5×10^6. Measurements were made of the steady-state heat flow from isothermal models near recovery temperature. The results can be summarized as follows:

1. Heat-transfer data for blunt shapes with laminar flow expressed as the Stanton number times the square root of Reynolds number (based on conditions behind a normal shock) are essentially independent of free-stream Mach number and body shape within the range of the present investigation.

2. If the Reynolds number is such that transition will occur somewhere on the body, bluntness can markedly reduce heat-transfer rates by increasing length of laminar run. Conversely, nose shapes having small radii of curvature in the shoulder region can cause early transition to turbulent flow and can greatly increase total heating rates.

3. The heat-transfer rate to a blunt shape was increased by concave stagnation regions having depths in excess of 0.3 nose diameter where large-scale unsteady flow can develop.

4. Stagnation point spikes up to 2 nose diameters in length caused substantial increases in heat-transfer rates for both steady and large-scale oscillating flow.

5. Heating rates over a flat-nosed, blunt shape are in fair agreement with theoretical estimates, although the extent to which large pressure gradients affect local heating rates remains, in part, uncertain.

Ames Research Center
National Aeronautics and Space Administration
Moffett Field, Calif., June 21, 1960

REFERENCES

1. Allen, H. Julian, and Eggers, A. J., Jr.: A Study of the Motion and Aerodynamic Heating of Missiles Entering the Earth's Atmosphere at High Supersonic Speeds. NACA TN 4047, 1957. (Supersedes NACA RM A53D28)

2. Reller, John O., Jr.: Heat Transfer to Blunt Nose Shapes With Laminar Boundary Layers at High Supersonic Speeds. NACA RM A57F03a, 1957.

3. Stine, Howard A., and Wanlass, Kent: Theoretical and Experimental Investigation of Aerodynamic-Heating and Isothermal Heat-Transfer Parameters on a Hemispherical Nose With Laminar Boundary Layer at Supersonic Mach Numbers. NACA TN 3344, 1954.

4. Carter, Howard S., and Bressette, Walter E.: Heat-Transfer and Pressure Distribution on Six Blunt Noses at a Mach Number of 2. NACA RM L57C18, 1957.

5. Stoney, William E., Jr.: Aerodynamic Heating of Blunt Nose Shapes at Mach Numbers up to 14. NACA RM L58E05a, 1958.

6. Chapman, Dean R.: A Theoretical Analysis of Heat Transfer in Regions of Separated Flow. NACA TN 3792, 1956.

7. Stalder, Jackson R., and Nielsen, Helmer V.: Heat Transfer From a Hemisphere-Cylinder Equipped With Flow-Separation Spikes. NACA TN 3287, 1954.

8. Crawford, Davis H.: Investigation of the Flow Over a Spiked-Nose Hemisphere-Cylinder at a Mach Number of 6.8. NASA TN D-118, 1959

9. Bogdonoff, S. M., and Vas, I. E.: Preliminary Investigations of Spiked Bodies at Hypersonic Speeds. Princeton University, Dept. of Aero. Engr., Rep. 142, 1958.

10. Hermach, C. A., Kraus, Samuel, and Reller, John O., Jr.: Reduction in Temperature-Recovery Factor Associated With Pulsating Flows Generated by Spike-Nosed Cylinders at a Mach Number of 3.50. NACA RM A56L05, 1957.

11. van Driest, E. R.: The Problem of Aerodynamic Heating. Aero. Engr. Rev., vol. 15, no. 10, Oct. 1956, pp. 26-41.

12. Sibulkin, M.: Heat Transfer Near the Forward Stagnation Point of a Body of Revolution. Jour. Aero. Sci., vol. 19, no. 8, Aug. 1952, pp. 570-571.

13. Lees, Lester: Laminar Heat Transfer Over Blunt-Nosed Bodies at Hypersonic Flight Speeds. Jet Propulsion, vol. 26, no. 4, Apr. 1956, pp. 259-269.

14. Cohen, Clarence B., and Reshotko, Eli: Similar Solutions for the Compressible Laminar Boundary Layer With Heat Transfer and Pressure Gradient. NACA Rep. 1293, 1956. (Supersedes NACA TN 3325)

TABLE I.- COMPARISON OF HEAT TRANSFER TO SHARP AND BLUNT 60° CONES

M_∞	d/D	St_a	St_b	$\frac{St_b \text{ at } d/D = 0.333}{St_b \text{ at } d/D = 0}$	Remarks
3.02	0	0.00398	0.00796	0.691	Partly turbulent B.L. ↓ Laminar B. L.
	.333	.00281	.00550		
3.50	0	.00255	.00510	.437	
	.333	.00114	.00223		
4.24	0	.00183	.00366	.844	
	.333	.00158	.00309		
5.05	0	.00282	.00564	.791	
	.333	.00228	.00446		
6.30	0	.00540	.01080	.795	
	.333	.00438	.00858		

$$\frac{\text{SURFACE AREA OF BLUNT CONE}}{\text{SURFACE AREA OF SHARP CONE}} = 0.979$$

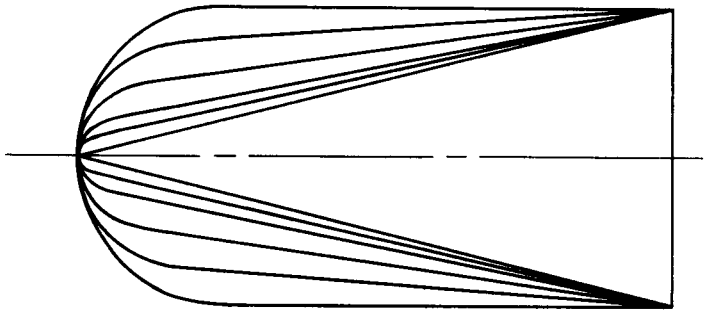

Group 1

1 Inch

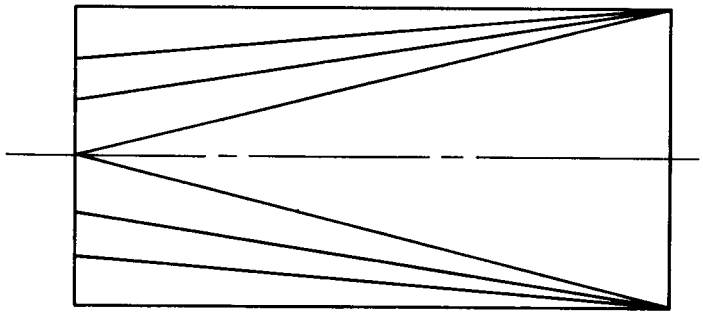

Group 2

(a) Hemisphere cones and truncated cones

Figure 1.- Shapes used in heat-transfer investigation.

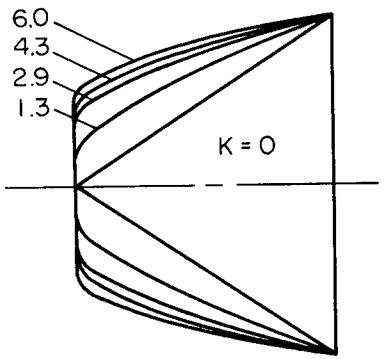

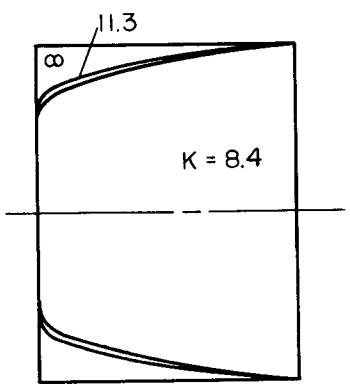

Group 3—constant L/D

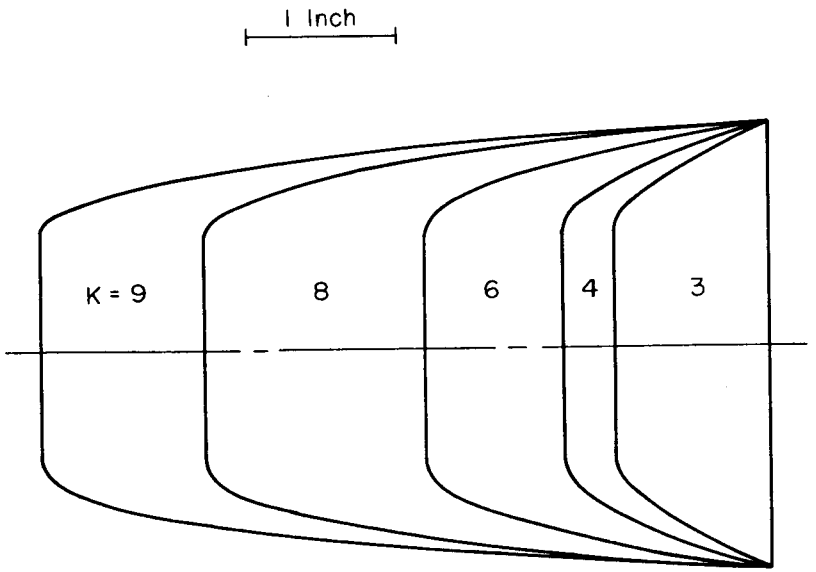

Group 4—constant d/D

(b) K-series shapes

Figure 1.- Continued.

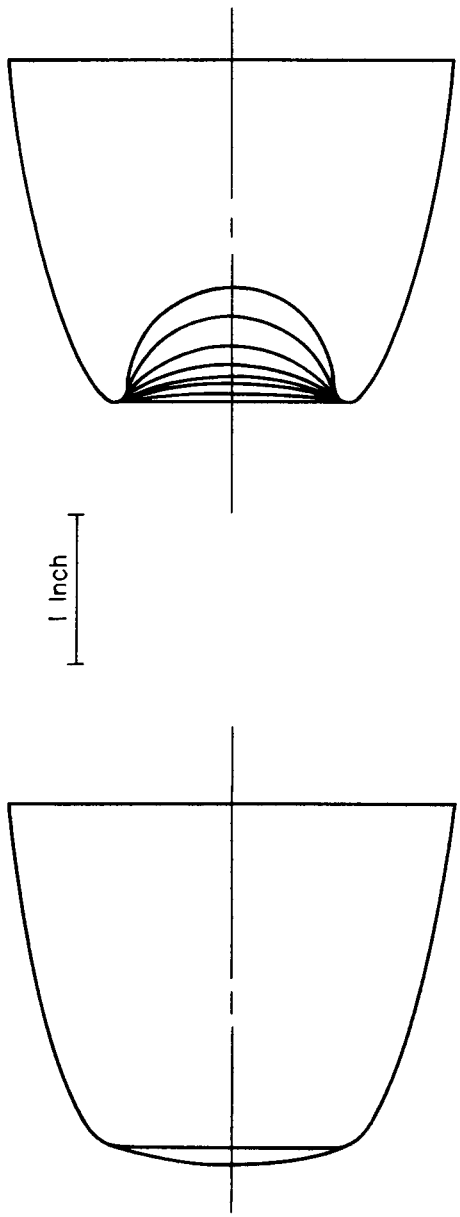

(c) Variable nose profile shapes.

Figure 1.- Continued.

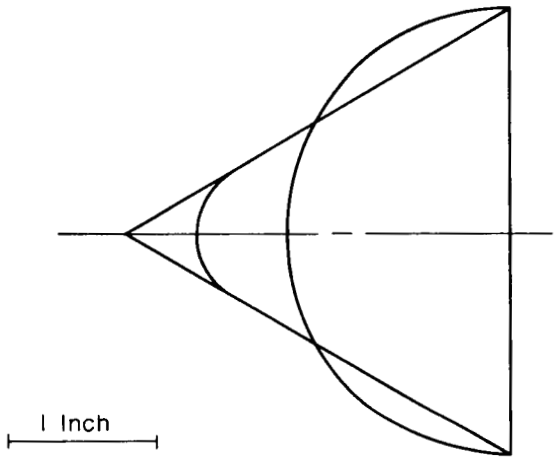

Group 6

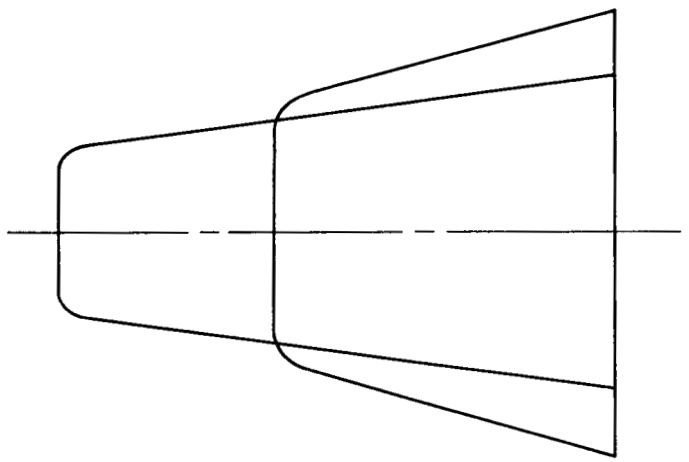

Group 7

(d) Reference and equal-surface-area shapes

Figure 1.- Continued.

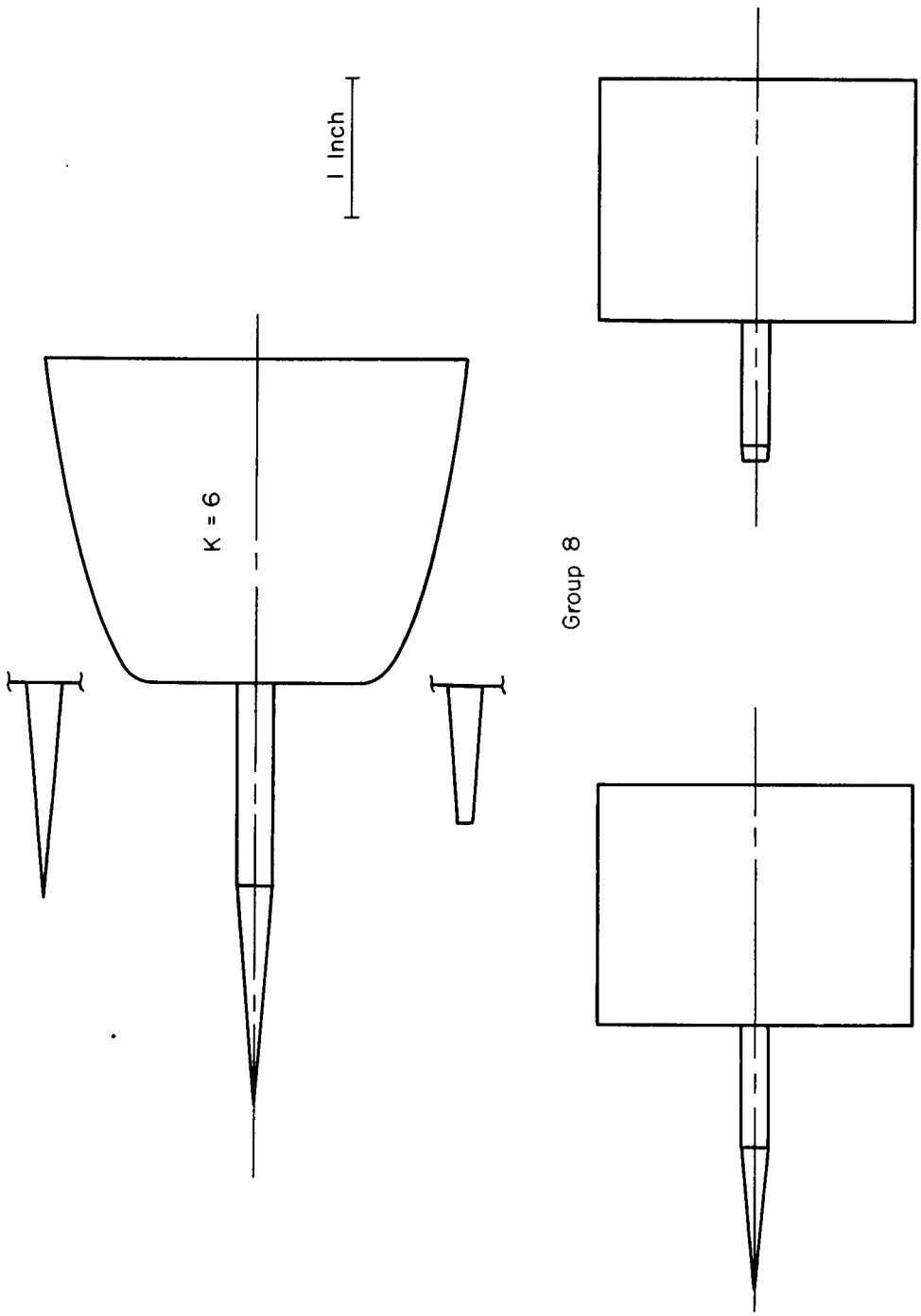

(e) Spiked shapes.

Figure 1.- Continued.

(f) Segments of K-6 shape

Figure 1.- Concluded.

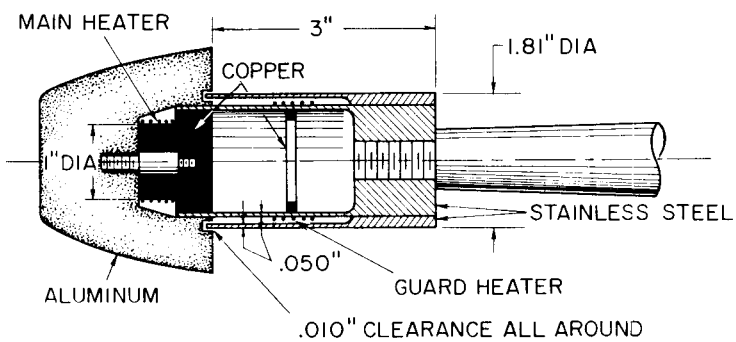

Figure 2.- Heat transfer apparatus.

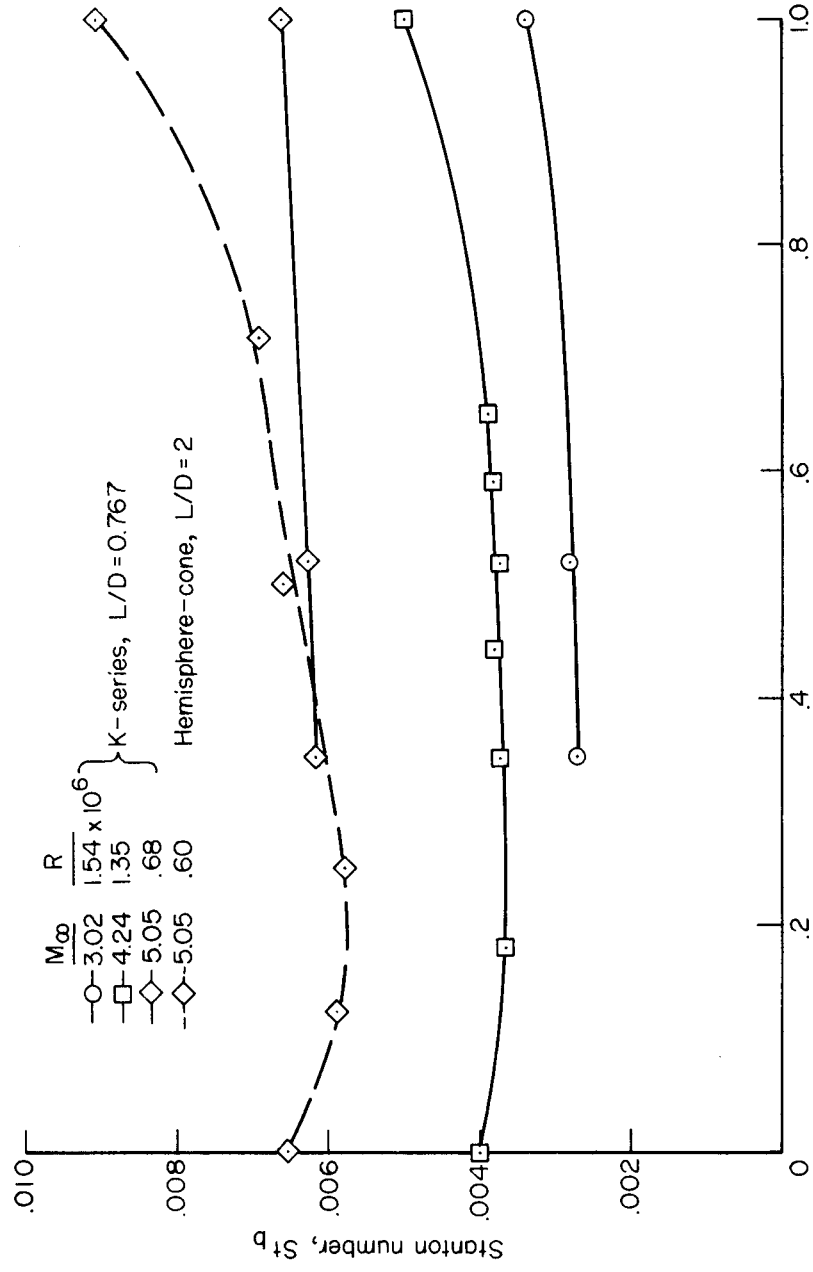

(a) Heat-transfer rates per unit base area.

Figure 3.- Effect of nose size on heat-transfer rate; laminar boundary layer.

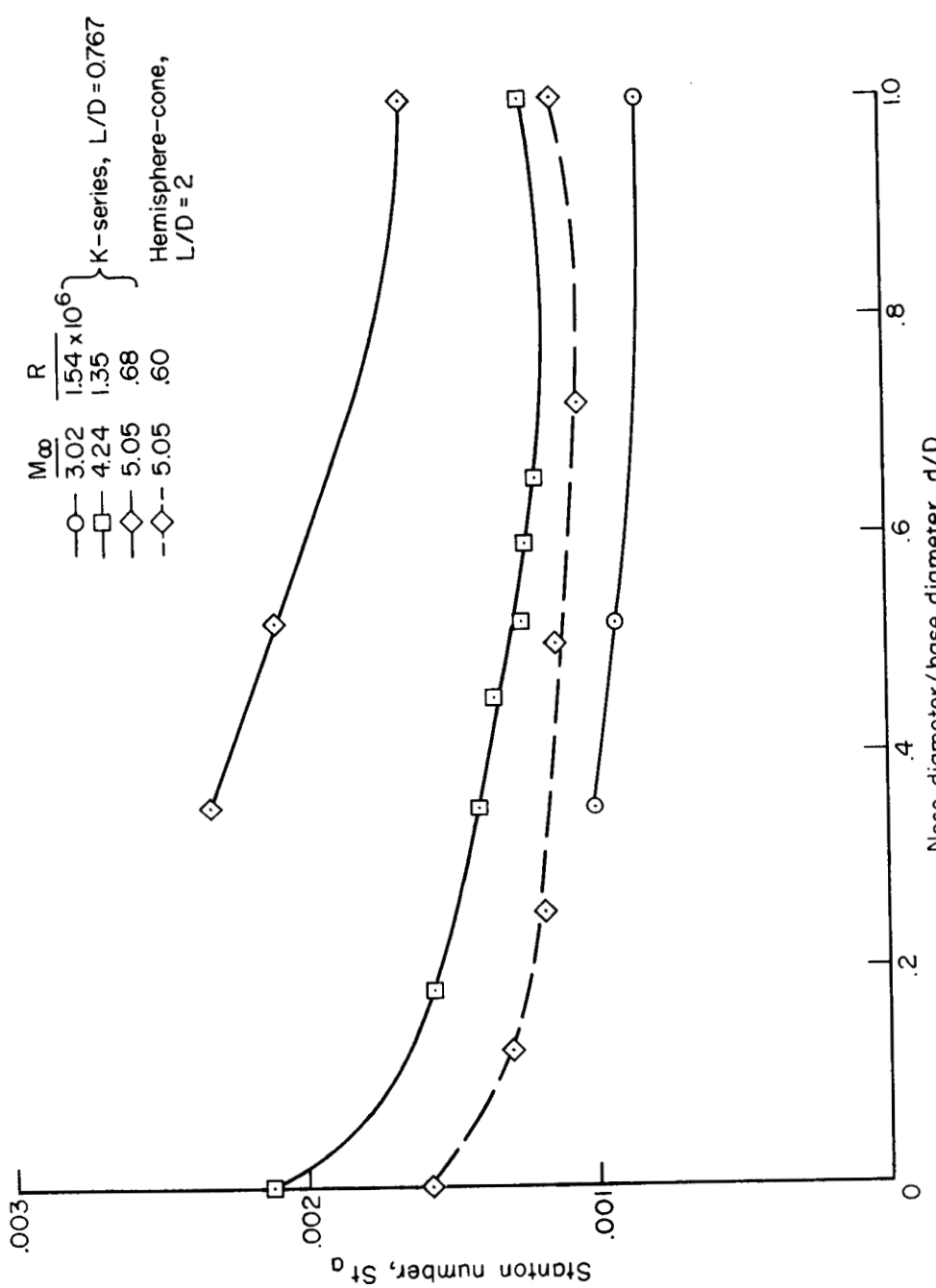

(b) Heat-transfer rates per unit surface area.

Figure 3.- Concluded.

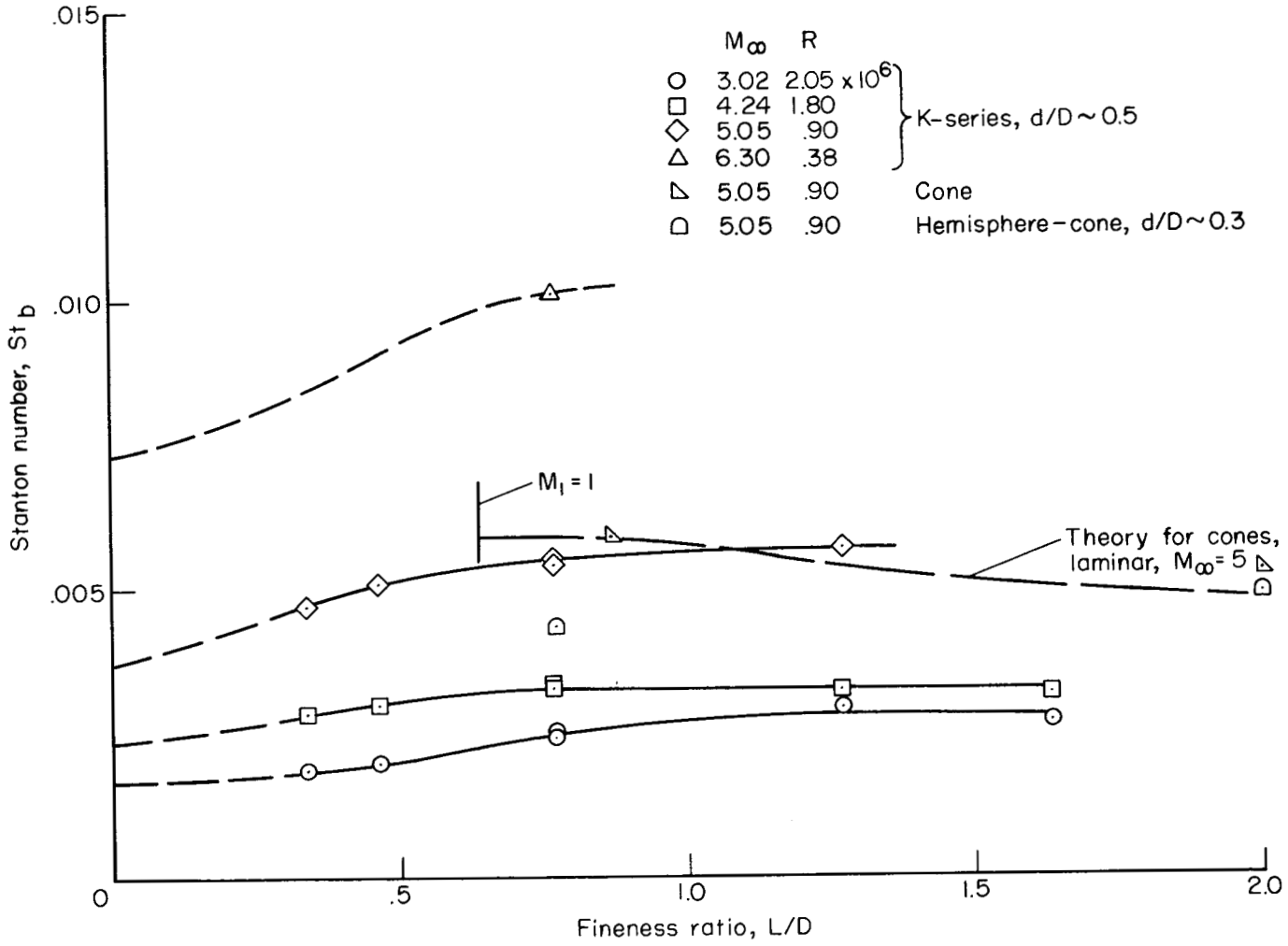

(a) Heat-transfer rates per unit base area.

Figure 4.- Effect of fineness ratio on heat-transfer rate; laminar boundary layer.

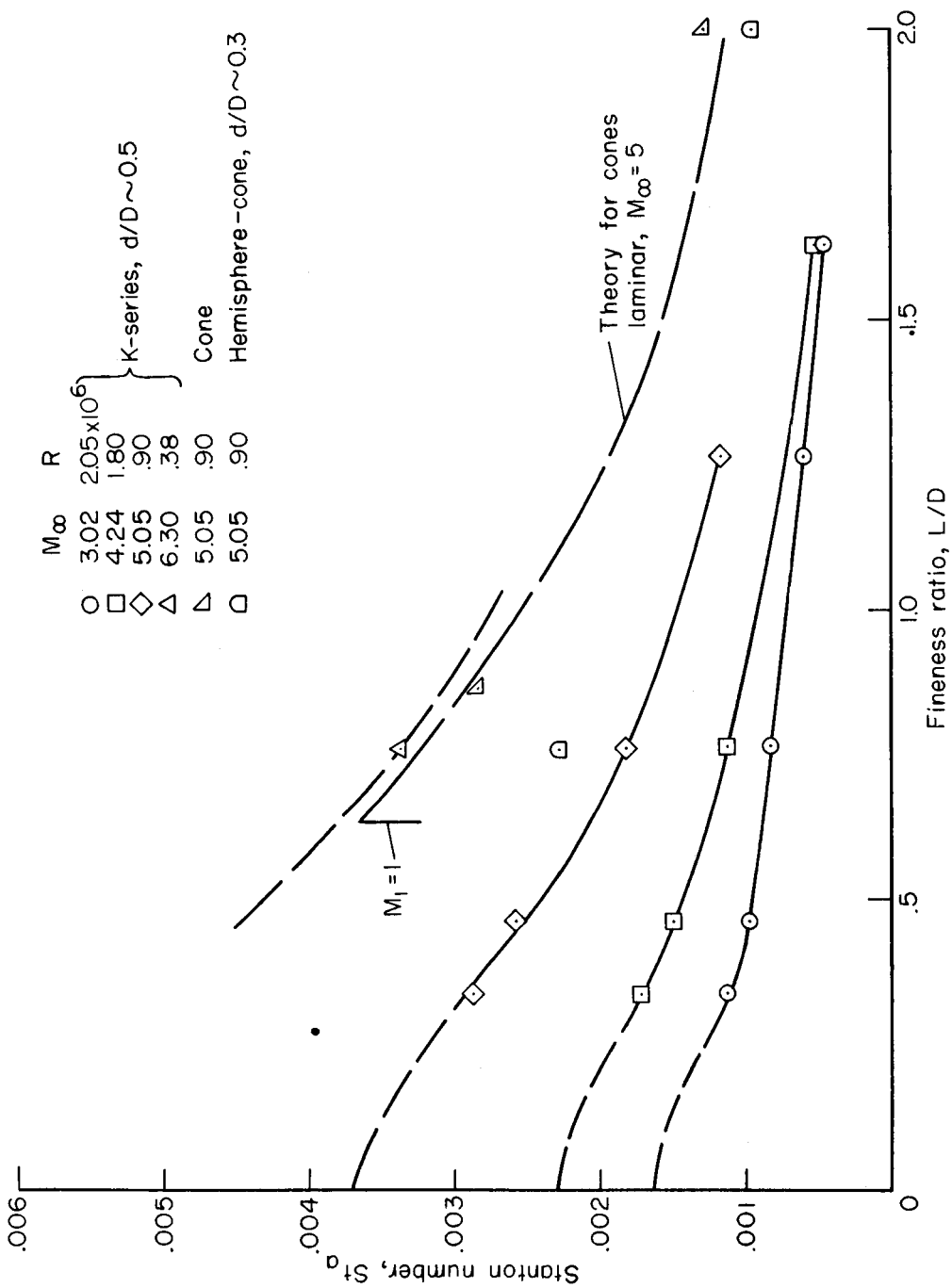

(b) Heat-transfer rates per unit surface area.

Figure 4.- Concluded.

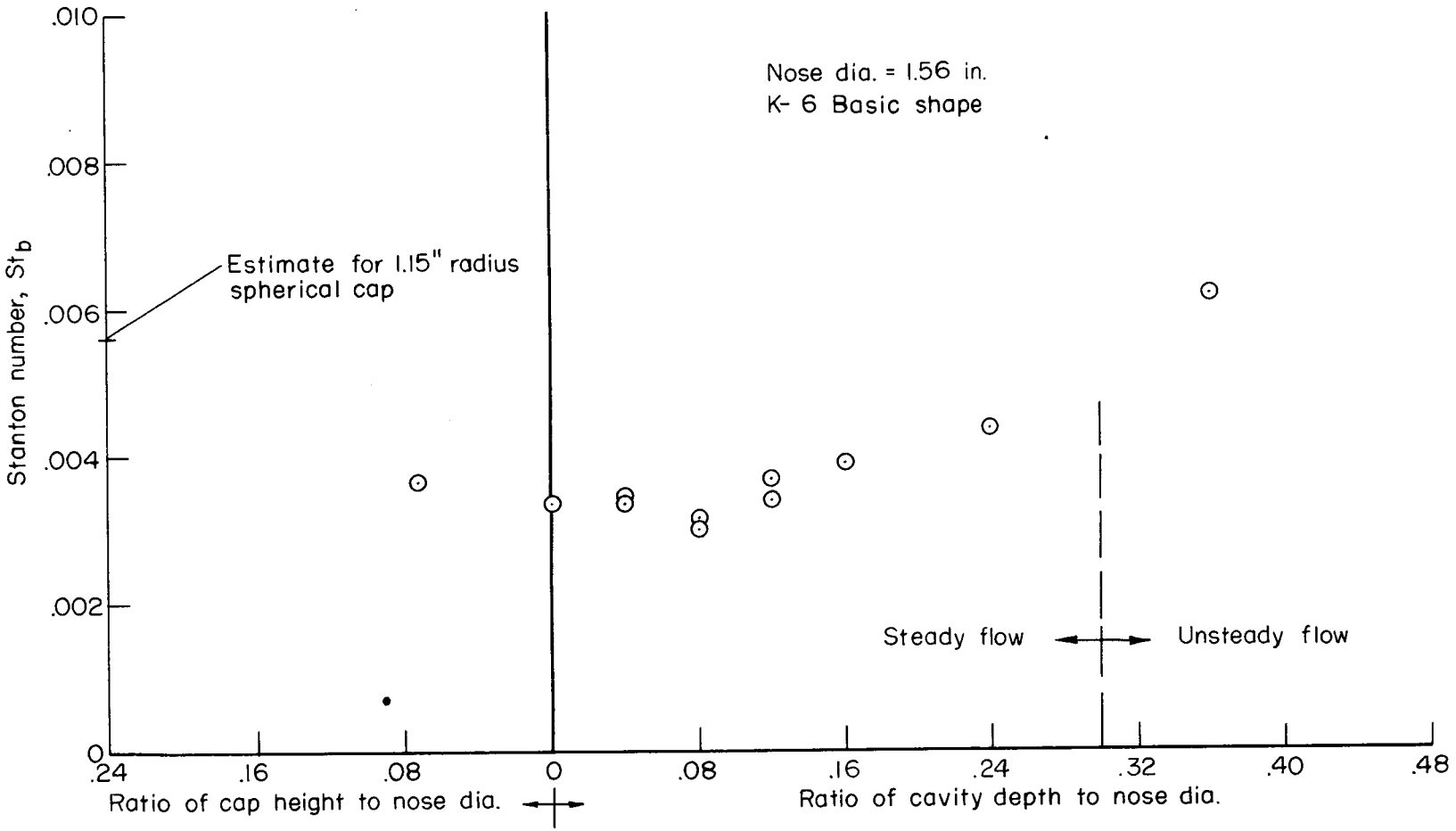

Figure 5.- Variation of heat-transfer rate with nose profile; $M_\infty = 4.24$, $R = 1.80 \times 10^6$.

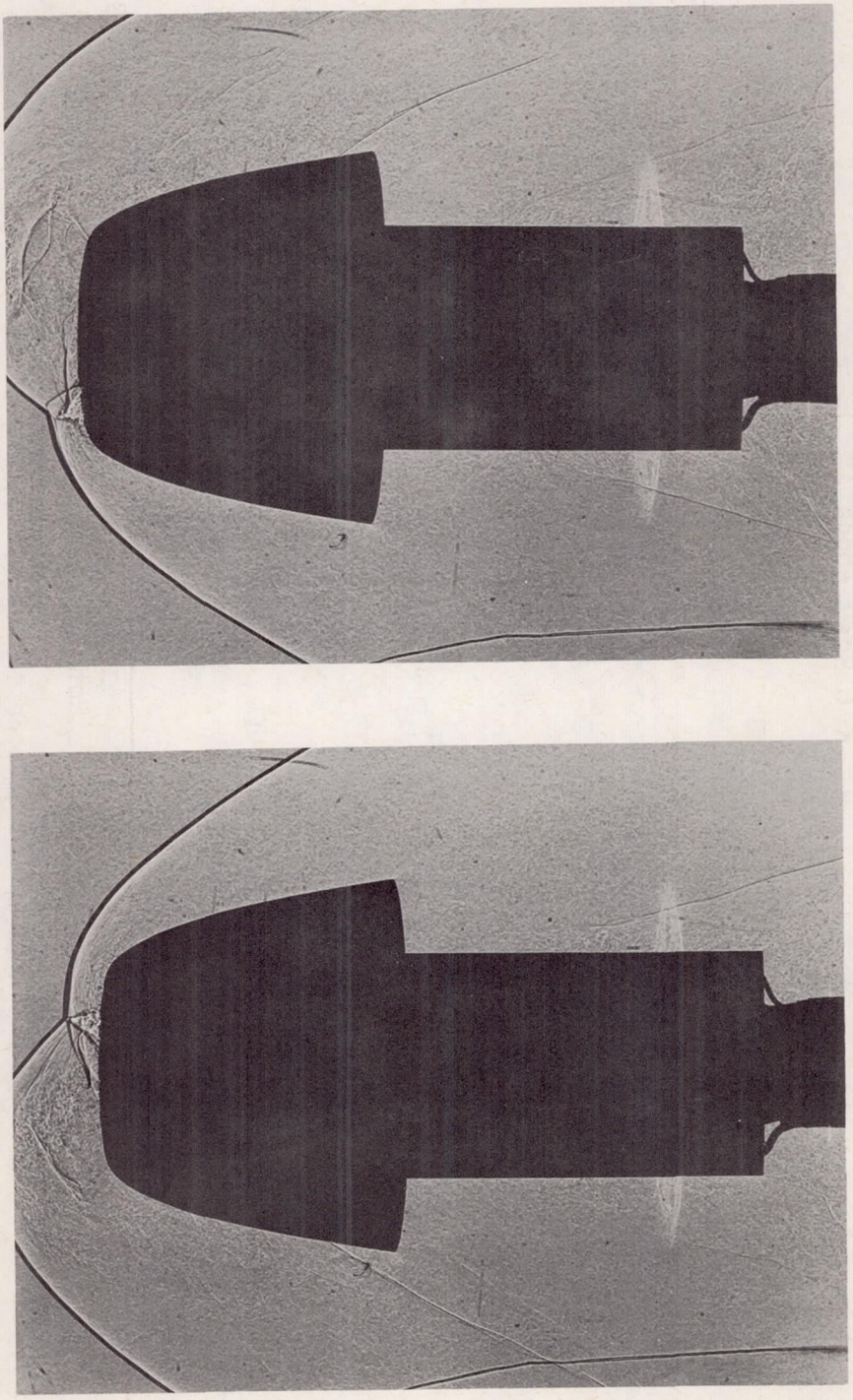

Figure 6.- Unsteady flow over K-6 shape with nose cavity; $M_\infty = 4.24$, $R = 1.80 \times 10^6$, ratio of depth to nose diameter of 0.36.

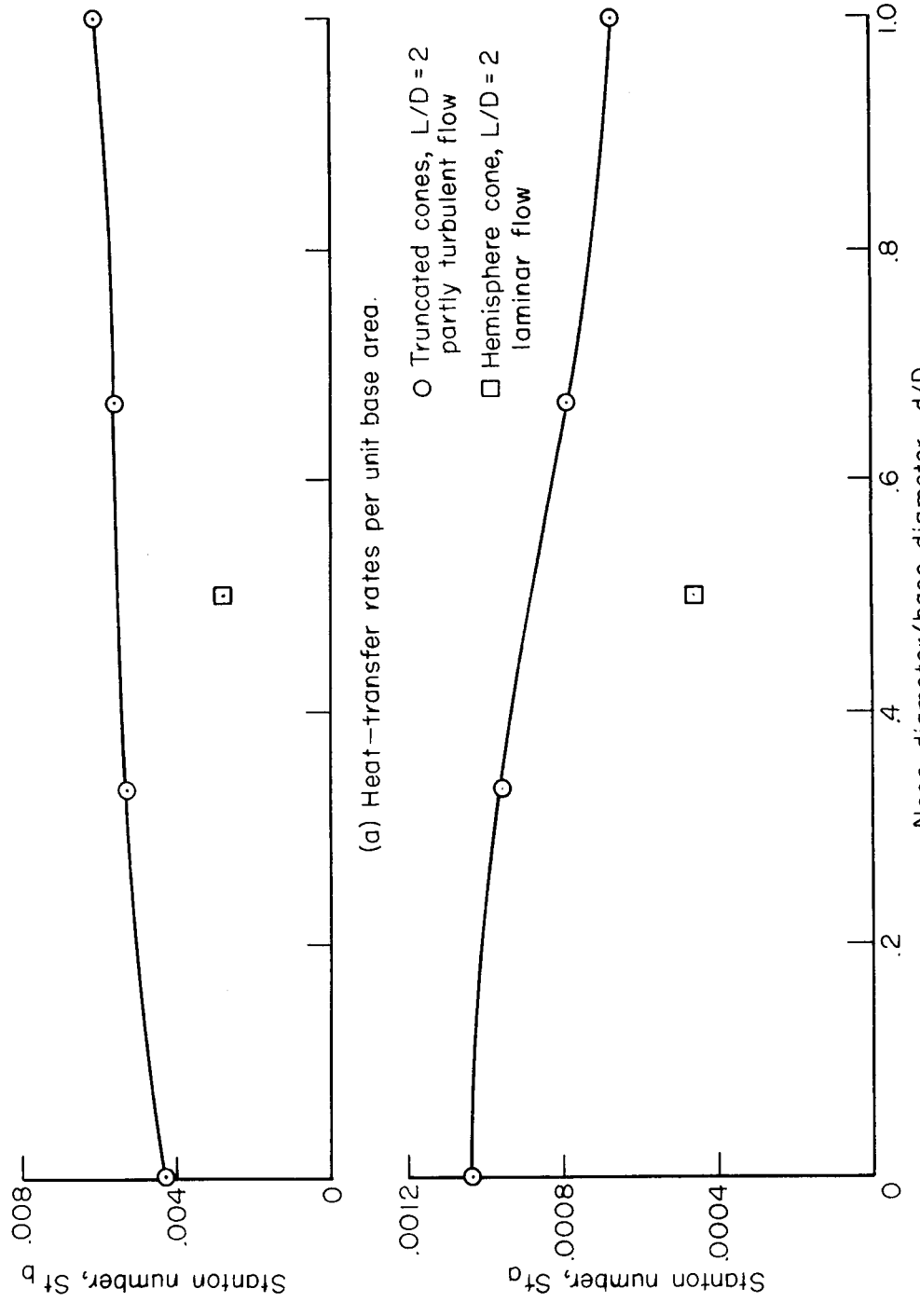

Figure 7.- Effect of boundary-layer transition due to body nose shape on heat-transfer rates; $M_\infty = 3.5$, $R = 1.64 \times 10^6$.

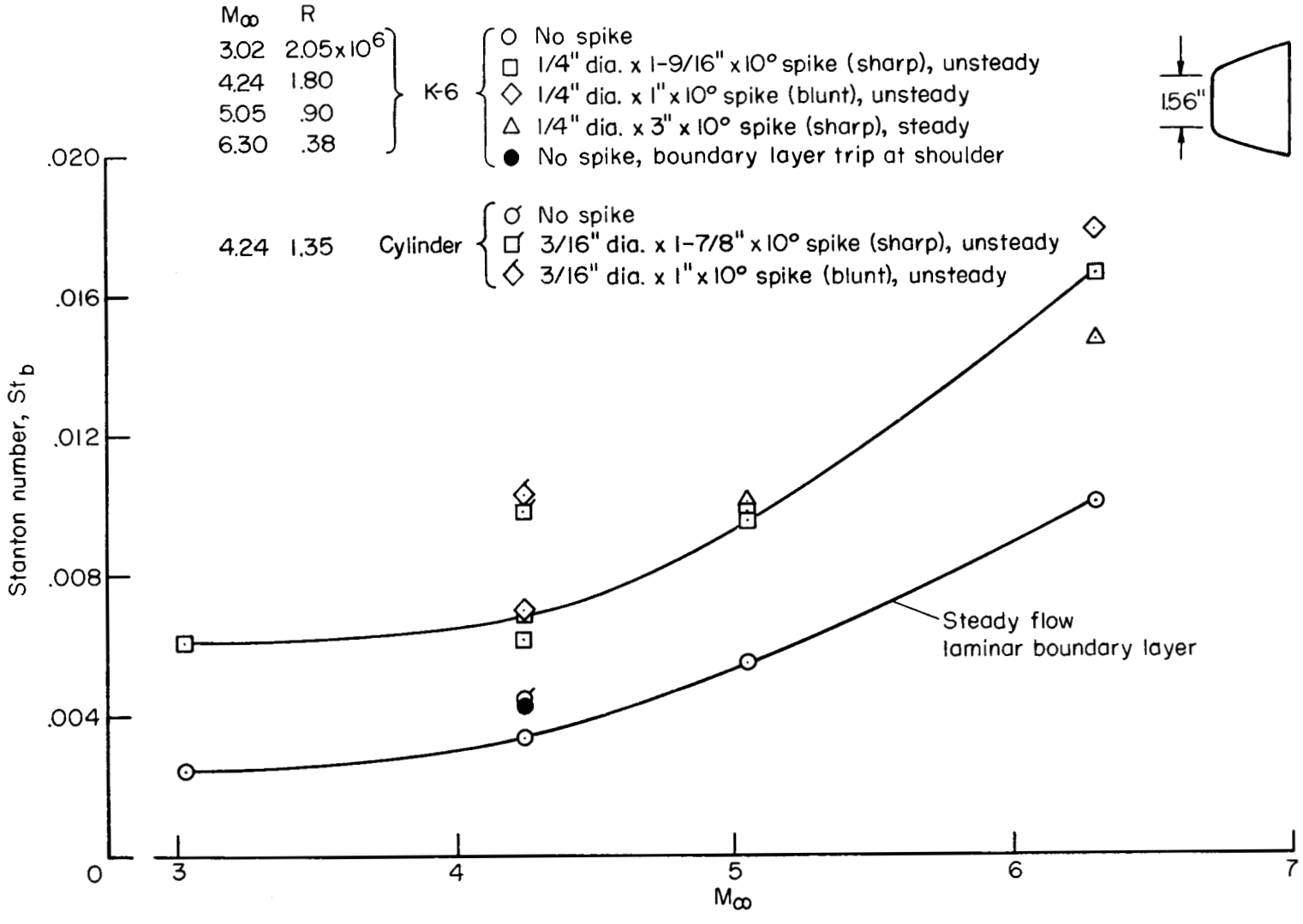

Figure 8.- Effect of nose spikes on heat-transfer rates.

CONFIDENTIAL

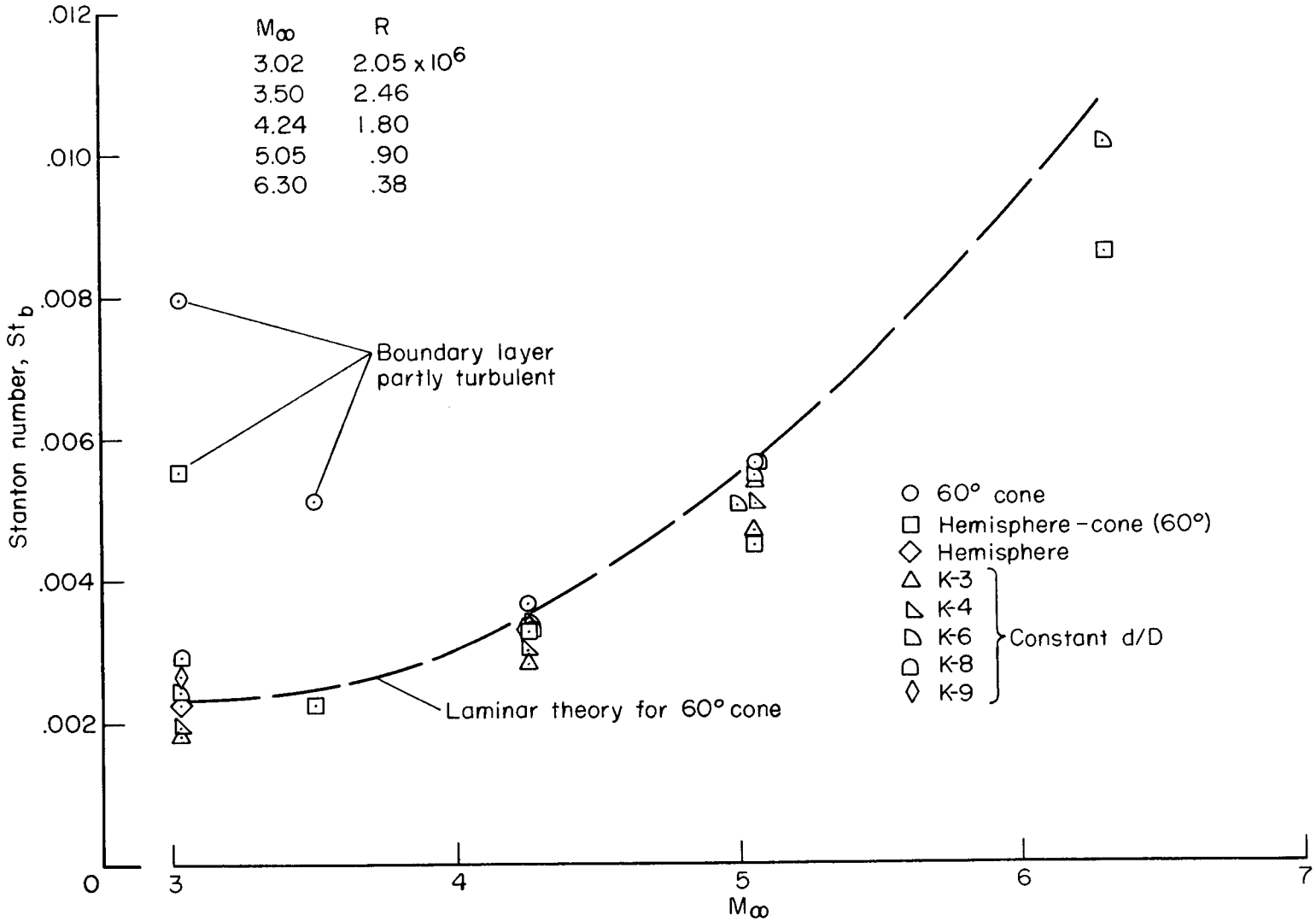

Figure 9.- Heat-transfer rates of K-series and reference bodies.

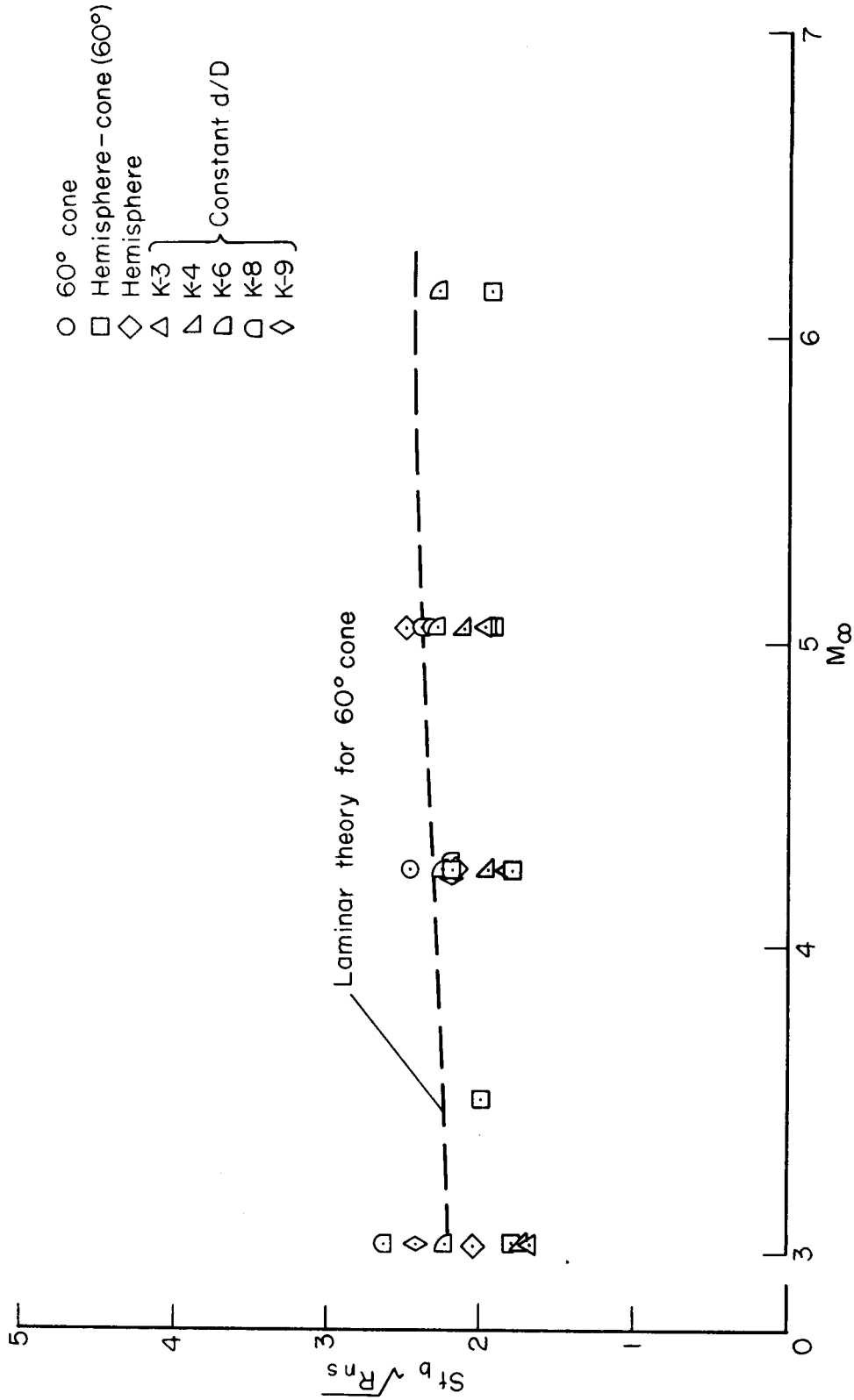

Figure 10.- Variation of heat-transfer parameter with Mach number.

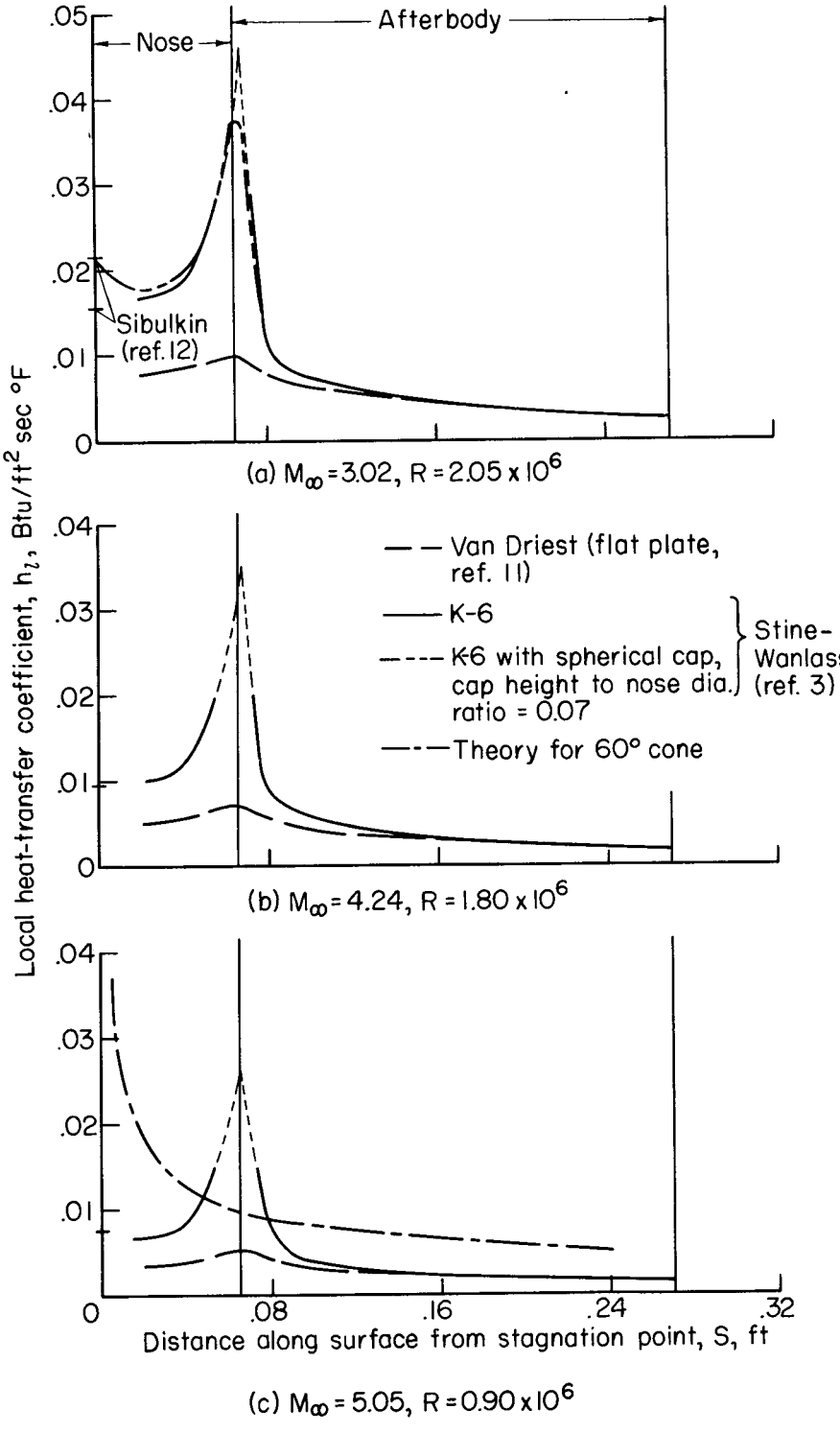

Figure 11.- Theoretical heat-transfer distribution over K-6 shape; laminar boundary layer.

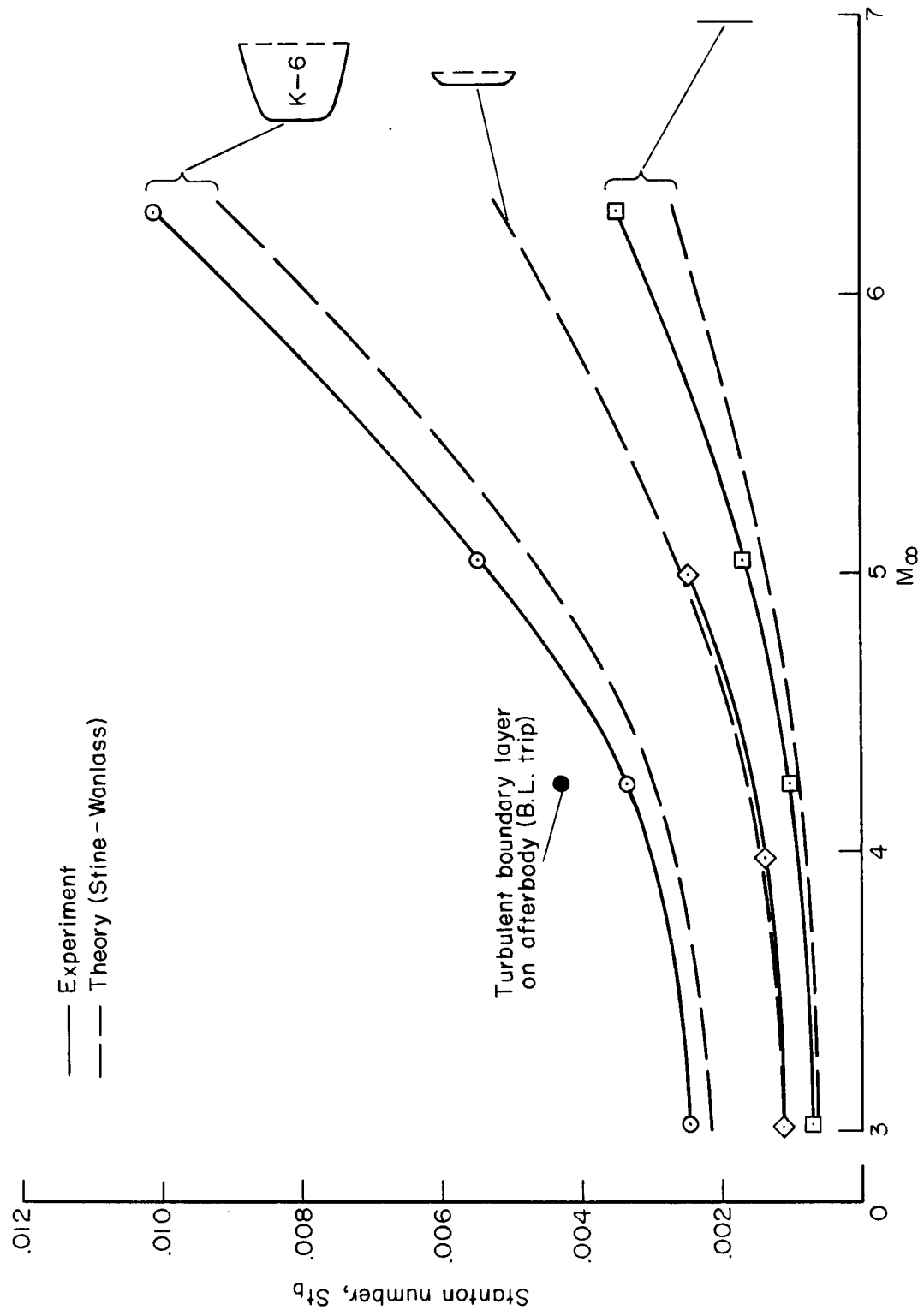

Figure 12.- Heat-transfer to a blunt body.

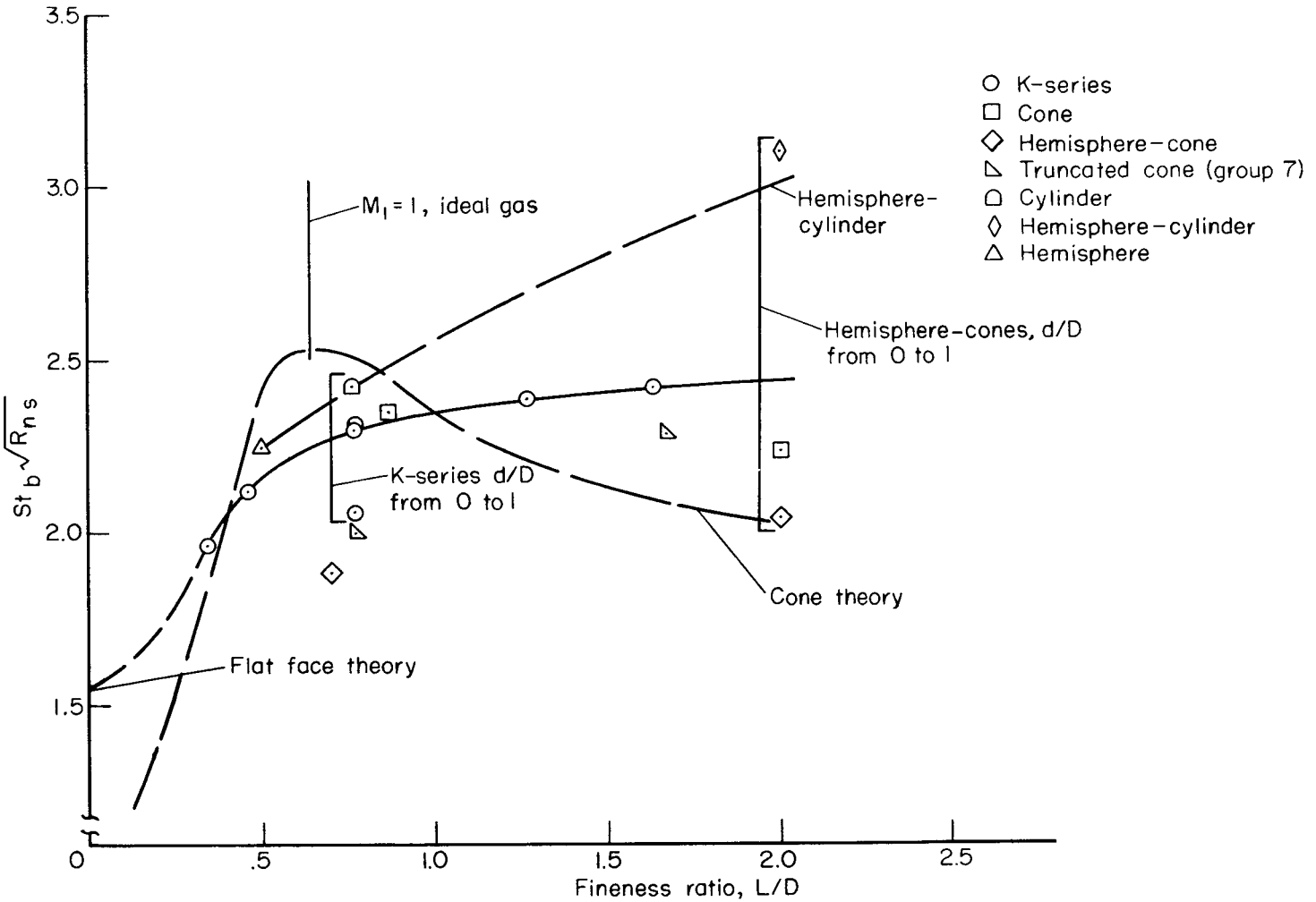

(a) Heat-transfer rate per unit base area.

Figure 13.- Heat-transfer summary, $M_\infty = 5.05$; laminar boundary layer.

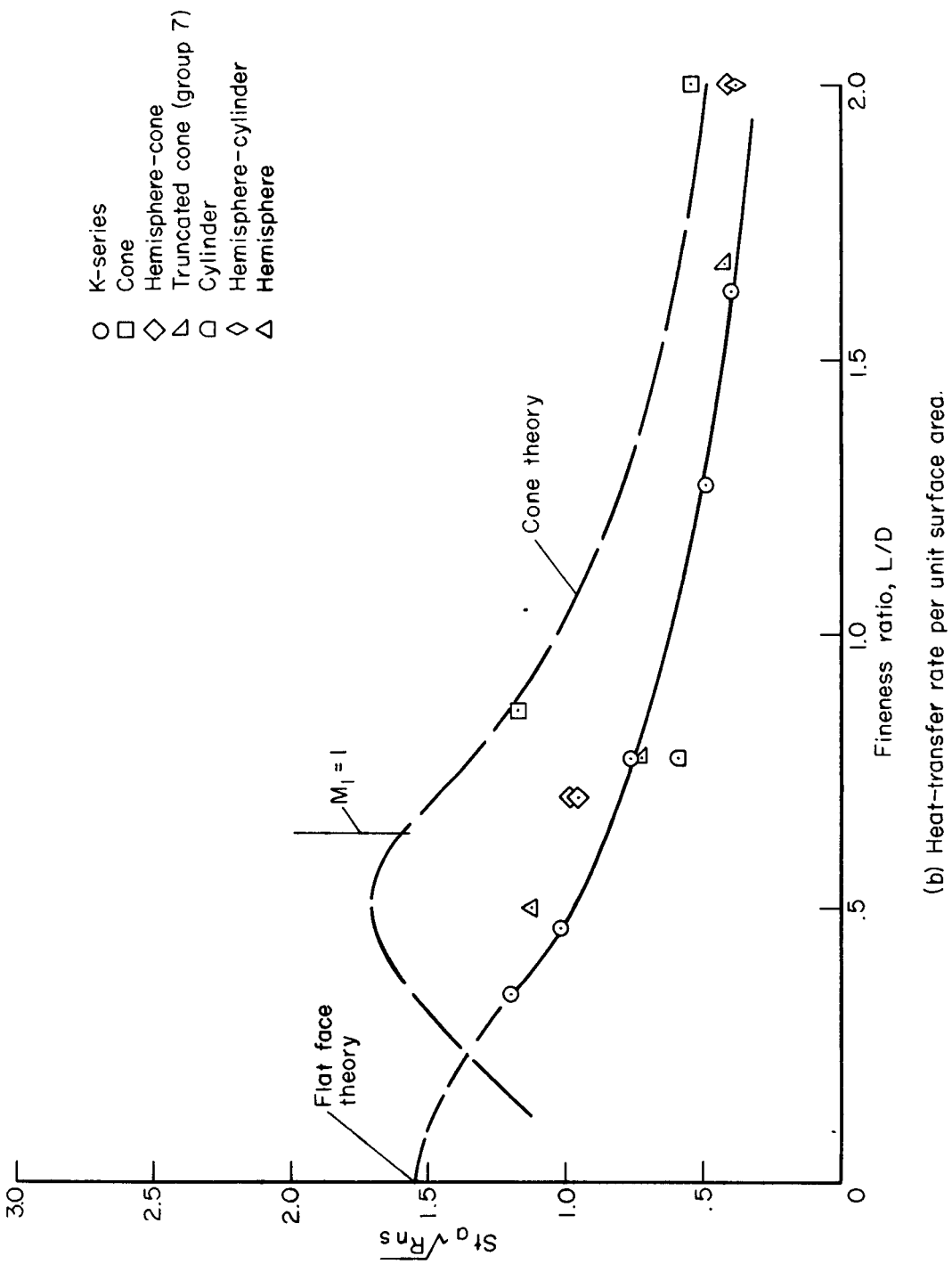

(b) Heat-transfer rate per unit surface area.

Figure 13.- Concluded.